Structural reliability analysis of offshore jackets for system-level fatigue design

Mendoza, Jorge; Nielsen, Jannie Sønderkær; Sørensen, John Dalsgaard; Köhler, Jochen

Published in:
Structural Safety

DOI (link to publication from Publisher):
10.1016/j.strusafe.2022.102220

Publication date:
2022

Document Version
Publisher's PDF, also known as Version of record

Structural Safety 97 (2022) 102220

Contents lists available at ScienceDirect

Structural Safety

journal homepage: www.elsevier.com/locate/strusafe

Structural reliability analysis of offshore jackets for system-level fatigue design

Jorge Mendoza [a,*], Jannie S. Nielsen [b], John D. Sørensen [b], Jochen Köhler [a]

[a] Norwegian University of Science and Technology, Department of Structural Engineering, 7491 Trondheim, Norway
[b] Aalborg University, Department of the Built Environment, 9220 Aalborg, Denmark

ARTICLE INFO

Keywords:
Jackets
System-level design
Reliability-based design
Fatigue
System reliability

ABSTRACT

Lattice systems such as offshore jackets and towers are weight-efficient support structures for wind energy and oil and gas units. Nevertheless, their light-weight is achieved at the expense of increasing their proneness to fatigue failure, due to their many welded connections. Consequently, special attention is to be dedicated to the design of the fatigue hot spots. System-level fatigue design methods aim at calibrating the reliability of the fatigue components to achieve a desired target system reliability. These methods rely on the accurate assessment of the system probability of failure, which is computationally demanding due to the statistical dependence among fatigue limit states and the large number of possible deterioration states that need to be taken into account. In the present paper, we develop a novel approach, called the truncation algorithm, to estimate lower and upper bounds of the system reliability due to extreme environmental and fatigue limit states within feasible computational time. The proposed approach is applied to assessing existing system-level fatigue design methods and to study system effects, such as the effects of redundancy and the correlation among fatigue limit states on the system reliability.

1. Introduction

Jackets and towers are bottom-fixed structures that are commonly used to support offshore units, such as oil and gas platforms and wind turbines, in shallow and intermediate waters. They are lattice structures made of tubular members, containing three or more legs and a bracing system connecting the legs. Offshore lattice structures are fatigue sensitive due to the induced cyclic environmental loading, which is predominantly caused by wave-induced drag and inertia forces, and to the large number of welded connections between tubular members. These welded joints are the fatigue-prone locations of the structure and are typically referred to as *hot spots* [1]. Because of the large costs associated with manufacturing and maintaining these joints within acceptable safety levels, the weight-efficiency of offshore lattice structures is not always associated with cost-efficiency [2]. Thus, the fatigue design of the joints should be further optimised in order to keep these structures competitive [3]. System-level fatigue design, understood here as the calibration of the fatigue reliabilities of the hot spots of a structure to achieve a given target system reliability, is a promising solution to further optimise the design of jacket structures. Note that the cross-section dimensions of the tubular members at the fatigue hot spots can be optimised given the target component reliabilities using available methods [3]. System-level fatigue design relies on the accurate estimation of the system reliability, which is computationally challenging. Existing methods to assess the system reliability and system-level fatigue design are reviewed in Sections 1.1 and 1.2.

1.1. Structural reliability assessment of jackets

The system reliability is to be assessed based on the relevant limit states, which are here assumed to be extreme environmental load and fatigue limit states. A typical assumption to assess the system reliability is that fatigue damage at a hot spot does not affect the structural response until it reaches a critical magnitude, after which point the hot spot and, consequently, the structural member containing the hot spot fail and no longer participate in load bearing [4]. This assumption is justified for offshore lattice structures subject to high-cycle fatigue because their predominant structural collapse mechanism is typically an extreme weather event [5]. Hence, the global resistance of the structure due to extreme environmental loading can be uncoupled from the fatigue deterioration processes at the hot spots. As a consequence, one just needs to know the fatigue state (failed or not failed) of all the members of the structure in order to assess the structural integrity of the deteriorated system. From a design point of view, the fatigue

* Corresponding author.
E-mail address: jorge.m.espinosa@ntnu.no (J. Mendoza).

https://doi.org/10.1016/j.strusafe.2022.102220
Received 11 August 2021; Received in revised form 23 March 2022; Accepted 24 March 2022
Available online 11 April 2022

condition of the hot spots is uncertain. Thus, it is required to integrate over the probability of occurrence of the possible deterioration states. The fatigue deterioration state of a structure with N fatigue-prone members at a given point in time t, denoted $\Psi(t)$, is thus a process that can take 2^N distinct realisations. The total probability theorem can be applied to compute the probability of system failure $P_{f,sys}(t)$ at time t:

$$P_{f,sys}(t) = \Pr\left(C(t)\right) = \sum_{p=0}^{2^N-1} \Pr\left(C|\psi_p\right) \Pr\left(\Psi(t) = \psi_p\right), \quad (1)$$

where C is the event of collapse or global failure of the structure, $\Pr\left(C|\psi_p\right)$ is the conditional probability of collapse due to an extreme load event of the deteriorated structure being associated with state ψ_p, and $\Pr\left(\Psi(t) = \psi_p\right)$ is the probability of occurrence of deterioration state ψ_p.

Typically, the probabilistic load model is chosen in reference to one year. In that case, $P_{f,sys}(t)$ is the so-called interval annual probability of system failure during the interval $(t-1, t]$, as defined by Straub et al. [6]. This failure probability does not take into account the fact that the system may have failed during any of the previous years, which is further discussed in Section 6. To assess the conditional failure probability terms, i.e., $\Pr\left(C|\psi_p\right)$ for $p = 0, 1, 2^N - 1$, it is common to assume that the fatigue loads are statistically independent from the extreme annual loads [5]. Furthermore, the ultimate structural resistance and the fatigue resistance of the structural members are assumed statistically independent. Given these assumptions, the ultimate load and fatigue limit states are uncorrelated.

The consideration of system effects, i.e., of the joint probability of occurrence of the fatigue failures $\Pr(\Psi(t))$, is of special relevance for the computation of the system reliability. Straub and Der Kiureghian [5] found that assuming the fatigue limit states of the different hot spots to be uncorrelated results in a large overestimation of the system reliability for purely parallel systems. Unfortunately, the consideration of system effects is computationally demanding. In fact, the exact computation of the system reliability from Eq. (1) is unfeasible for most realistic structural systems, even if the fatigue deterioration processes are assumed to be uncorrelated. This is due to the large number of combinations of possible deterioration states that need to be assessed, which grows exponentially with the number structural members (2^N). Nevertheless, if the assumption of uncorrelated fatigue processes would hold true, it would be possible to approximate the system reliability without incurring much error. An example of such approximation was proposed by Moan [7]:

$$P_{f,sys}(t) \approx \Phi(-\beta_{sys,0}) + \sum_{i=1}^{N} \Phi(-\beta_{M,i}(t)) \cdot \Pr(C|\bar{F}_1 \cap \cdots \cap \bar{F}_{i-1} \cap F_i \cap \bar{F}_{i+1} \cap \cdots \cap \bar{F}_N), \quad (2)$$

where $\Phi(\cdot)$ is the standard normal cumulative distribution function, $\beta_{sys,0}$ is the reliability index of the intact system, $\beta_{M,i}$ is the cumulative fatigue reliability index of member i, F_i is the event of fatigue failure of member i, and a superposed bar indicates the complementary event. According to the equation, the failure probability of the deteriorated system is computed as the sum of the intact probability of system failure and the contributions of the deterioration states with only one failed member at a time, which are here denominated first-member-failure deterioration states. In the equation, the probabilities of occurrence of the first-member-failure deterioration states are approximated by the cumulative probabilities of occurrence of fatigue failure of the members.

Eq. (2) has been often used in practical applications, see e.g., [8–10], and it is part of a recommended practice guideline by the Health & Safety Executive (HSE), see [11]. For clarity, we refer to this approximation as the HSE approximation. According to [9], the HSE approximation is based on two main assumptions: (i) considering full independence leads to conservative estimates; and (ii) the contribution of the deterioration states with one component failed at a time largely amounts to the totality of the probability of system failure. As already discussed, [5] showed that the first assumption is not necessarily true. The second assumption is supported, according to [9], by the observed low correlation among fatigue failures [12,13]. However, whereas fatigue failure events are practically uncorrelated, the investigation conducted by Maljaars and Vrouwenvelder [14] showed that the fatigue limit states are highly correlated. The compatibility of both facts can be easily demonstrated numerically. In Appendix A, the authors show that setting the pair-wise correlation among fatigue safety margins to 0.5 and using fatigue reliabilities in the order of magnitude of those dictated by offshore standards (such as DNVGL-RP-C203 [15] and NORSOK N-004 [16]) leads to a much smaller correlation coefficient among fatigue failures, approx. 0.06. Because the assumptions of the HSE approximation are not generally satisfied, the validity of applying the HSE method for the fatigue design of jacket-type structures should be further studied.

Alternatives to the HSE approximation have been proposed in the literature. Gharaibeh et al. [17] proposed to group members that similarly contribute to ultimate resistance in order to reduce the number of deterioration states to be assessed. However, to assess the grouping before actually computing the conditional probabilities of system failure requires expert judgement and may lead to judgement errors. Another approach, proposed by Kim et al. [18], consists in approximating the system reliability by considering a limited number of failure modes that are previously identified as main contributors to the probability of failure. Although this approach could potentially be applied to the assessment of deteriorating systems, its efficiency would be low, because the contributions of the different failure modes depend on both the fatigue design of the hot spots and time. Furthermore, in the context of optimisation, it is computationally advantageous to pre-compute the conditional probabilities of failure given the deterioration limit states so that it can be reached at any point of the optimisation. Thus, the authors consider that there is a need to efficiently and accurately approximate the system reliability as defined in Eq. (1).

1.2. System-level fatigue design methods

System-level methods for fatigue design have been developed in the literature [11,5]. The HSE guideline suggests to design the fatigue reliabilities of the hot spots by ensuring that all the summation terms in Eq. (2) are equal [11], i.e., that all structural members equally contribute to the system probability of failure. We refer to this approach as the HSE design method in this article. Another system-level fatigue design method was proposed by Straub and Der Kiureghian [5]. In their framework, a system consisting of fatigue hot spots is idealised with so-called equivalent Daniels systems (EDS), which are used for each hot spot to model its influence on the true system. The EDS models are parametrised as a function of two system-level characteristics, namely the number of hot spots and the redundancy of the system given failure of each of the hot spots. In this article, we refer to this approach as the EDS method. The application of the EDS method is explained in more detail in Section 4. Compared to the HSE design method, the EDS method has the benefit of considering the correlation among fatigue limits states. In [5], they demonstrate the validity of the EDS method with a case study. However, it has not been studied whether the method is valid regardless of the level of redundancy of the structure.

1.3. Aim and organisation of the article

The present article aims at developing a method, namely the truncation algorithm, to assess upper and lower bounds of the failure probability for jacket systems. The truncation algorithm is then used to estimate the implicit safety level associated with the HSE and EDS design methods and to study system effects for common jacket bracing systems. Specifically, the effects on the system reliability of the

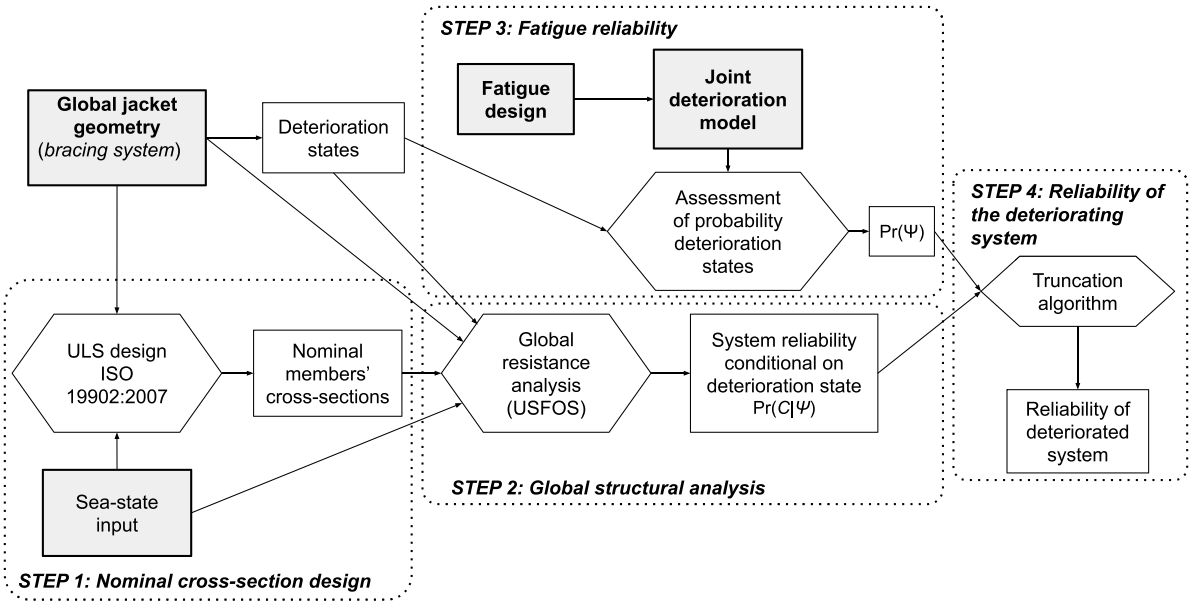

Fig. 1. Diagram of the steps followed to compute the system reliability. Grey boxes denote inputs; white rectangular boxes denote results; and hexagons denote computations.

correlation among fatigue limit states and the member reliabilities are studied.

First, a framework to assess the structural reliability of offshore lattice structures is presented in Section 2. The truncation algorithm is formally introduced in Section 3. The assessment of the implicit safety level associated with the HSE and EDS design methods for jacket systems is described in Section 4. The results of the study are presented in Section 5 and discussed in Section 6. The contributions of the article and the general conclusions are summarised in Section 7.

2. System reliability framework

The employed framework for assessing the system reliability of offshore lattice systems is summarised in Fig. 1. The analysis consist of four main parts:

- Step 1: design of the nominal cross-section dimensions of the members for given sea-state input. The structural members are designed based on ULS, according to ISO 19902:2007 [19].
- Step 2: evaluation of the global resistance of the structure designed in step 1 against extreme loads by means of non-linear pushover analyses. Analyses are conducted for the structure conditional on the different deterioration states Ψ and the results are ultimately used to assess the conditional system reliabilities $\Pr(C|\Psi)$.
- Step 3: computation of the probabilities of occurrence of the deterioration states $\Pr(\Psi)$, which are a function of the number of fatigue hot spots and the joint deterioration model. The former depends on the bracing system, and the latter depends on the fatigue design of the hot spots and the dependence among fatigue limit states.
- Step 4: computation of the system reliability based on the pre-computed conditional system reliabilities from step 2 and the probability of occurrence of the different deterioration states from step 3, see Section 2.3. As indicated in Fig. 1, this step can be computationally reduced with the truncation algorithm presented in Section 3.

Note that step 2 is necessarily conducted after step 1, and that step 4 is necessarily the last step. However, due to the considerations elaborated on in the previous section, step 3 can be conducted independently from steps 1 and 2. The assessment is conducted for various

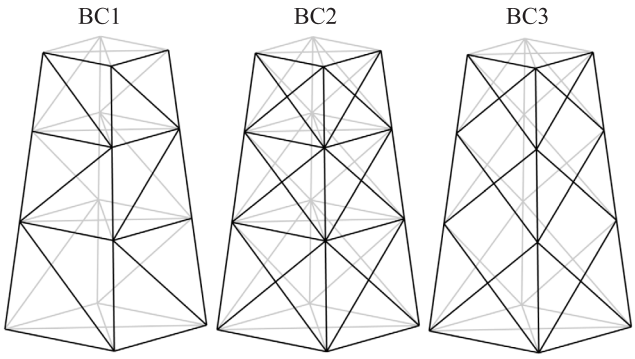

Fig. 2. Considered bracing configurations. BC1 is a K-bracing jacket and BC2 and BC3 are X-bracing jackets. Note that, as opposed to BC3, BC1 and BC2 have horizontal bracing separating the three bays.

bracing systems. Fig. 2 shows the considered bracing systems, denoted BC1, BC2 and BC3. These systems consist of combinations of K- and X-joints, which constitute some of the most typical configurations for offshore jackets and towers [20]. Their global dimensions, together with the employed inputs and the description of the nominal cross-section design approach and the ultimate resistance assessment are summarised in Appendix B, since these assessments are not the main focus of the article. The assessment of the conditional system reliability given a deterioration state is presented in Section 2.1. The assessment of the probability of occurrence of the deterioration states is presented in Section 2.2. The assessment of the unconditional system reliability is described in Section 2.3.

2.1. Conditional system reliability

The assessment of the conditional system reliability given a deterioration state is based on the probabilistic model used as background of ISO 19902:2007, which is reported by Efthymiou et al. [21,22]. In the probabilistic model, the ultimate resistance of the structure R and the annual maximum base shear E are lognormal distributed random variables with mean value R_m and E_m and coefficient of variation V_R and V_E, respectively.

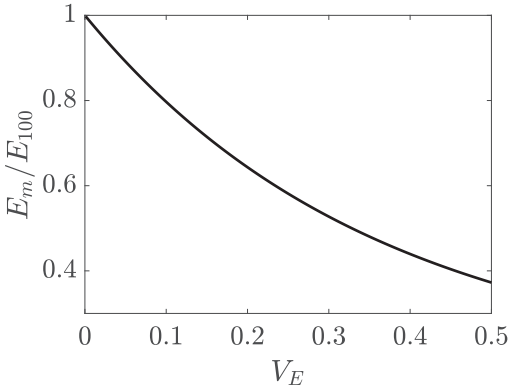

Fig. 3. Ratio between the mean yearly base shear E_m and the 100 year return base shear E_{100} as a function of the coefficient of variation of the environmental load.

The variability of the ultimate resistance depends on the variability of the failure mechanisms that are triggered until global failure. This variability might be complex to assess. Efthymiou et al. [21] propose to use a coefficient of variation $V_R = 0.05$ as a simplification. Another alternative, proposed in [22], is to estimate V_R as a function of the coefficient of variation of a member $V_{R,member}$, which they estimate as 10%, and the number of triggered parallel failure mechanisms N_F. This second approach leads to the following equation $V_R = V_{R,member}/\sqrt{N_F}$. In the present study, we assume $N_F = 2$, which leads to $V_R \approx 0.07$. This assumption is employed as a reasonable simplification based on the observed behaviour of global failure in the numerical simulations and because it does not have a significant impact on the conclusions drawn in the study. As mentioned above, the mean resistance R_m is estimated using pushover analysis. Note that the mean resistance can be zero for statically unstable structures, in which case the resistance is assumed to be deterministic with value $R = R_m = 0$.

For consistency with the loads used for design in Appendix B.1, we calibrate the mean maximum annual base shear E_m to represent the 100 year base shear. Let μ_E and σ_E be the parameters of the lognormal distribution of the load, F_E^{-1} be the inverse cumulative distribution of the load, $\Phi^{-1}(\cdot)$ be the inverse standard normal distribution function, and p_{100} be the fractile associated with a 100 year return period, i.e., $p_{100} \approx 0.99$. We can compute E_{100} as

$$E_{100} = F_E^{-1}(p_{100}) = \exp(\Phi^{-1}(p_{100}) \cdot \sigma_E + \mu_E). \tag{3}$$

The parameter σ_E can be directly computed from the coefficient of variation of the load as $\sigma_E = \sqrt{\ln(1+V_E^2)}$. Then, the parameter μ_E can be expressed as a function of E_{100}:

$$\mu_E = \ln(E_{100}) - \Phi^{-1}(p_{100}) \cdot \sqrt{\ln(1+V_E^2)}. \tag{4}$$

The mean annual environmental base shear can then be related to E_{100} as

$$E_m = E_{100} \exp\left(\left[\frac{1}{2}\sqrt{\ln(1+V_E^2)} - \Phi^{-1}(p_{100})\right] \cdot \sqrt{\ln(1+V_E^2)}\right). \tag{5}$$

The ratio E_m/E_{100} is plotted as a function of V_E in Fig. 3. The coefficient of variation of the load is set to $V_E = 0.35$ as a reasonable value [5,23] for the calculations in this investigation, leading to $E_m \approx 0.48 E_{100}$.

The described probabilistic model is used to assess the reliability index of the system conditional on a deterioration state ψ, denoted $\beta_{sys}(\psi)$, which is given by

$$\beta_{sys}(\psi) = \frac{\ln\left(\frac{R_m(\psi)}{E_m}\sqrt{\frac{1+V_E^2}{1+V_R^2}}\right)}{\sqrt{\ln[(1+V_R^2)(1+V_E^2)]}}, \tag{6}$$

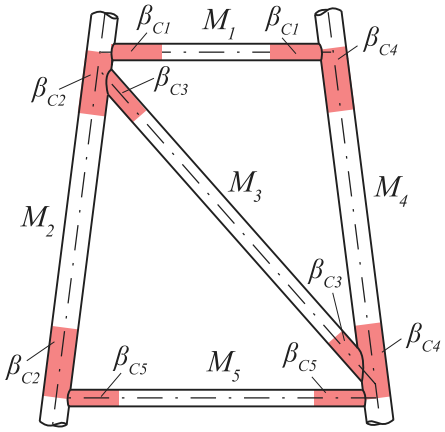

Fig. 4. Subsystem conformed by five structural members $M_1, \ldots, M_5$, each containing two fatigue-prone areas or hot spots (shaded areas). The hot spots of a given member M_i are associated with reliability indices β_{C_i}.

where $R_m(\psi)$ is the mean ultimate resistance of the system for a given deterioration state ψ.

Since the load is modelled using a reference period of one year, the reliability index β_{sys} is an annual reliability index. The distribution of the annual maximum load is typically assumed to be constant with time [5]. This assumption allows us to model the annual system reliability index conditional on a deterioration state as time invariant. Moreover, the mean ultimate resistance is assumed to be independent of the deterioration state as a simplification.

Given $\beta_{sys}(\psi)$, the annual probability of system failure conditional on a deterioration state is computed as

$$\Pr(C|\psi) = \Phi(-\beta_{sys}(\psi)). \tag{7}$$

2.2. Fatigue reliability

In this section, we present a method to compute the probability of occurrence of the different deterioration states Ψ. We consider a lattice structure with N members. Let the different structural members $M_1, M_2, \ldots, M_N$ contain each an arbitrary number of hot spots $n_1, n_2, \ldots, n_N$, respectively. Moreover, let the hot spots of a given member M_i be equally reliable, with cumulative reliability index β_{Ci}. These reliability indices are defined from a fatigue limit state function in accordance with [5]. The employed nomenclature is summarised in Fig. 4, where the fatigue hot spots are highlighted with colour. Here, the definition of hot spot is meant to encompass all the fatigue critical locations for a given member and joint, which implies that a member contains two hot spots. Nevertheless, the formulation is left open to the possibility of considering various critical locations per member and joint. Lastly, let the pair-wise correlation coefficient among the fatigue safety margins of all hot spots be ρ_M for all cases. The reliability indices of the hot spots and the pair-wise correlation coefficients fully characterise the probability mass function of Ψ for linear (or linearised) fatigue limit states.

It is assumed that a member fails due to fatigue if one or more of its fatigue hot spots fail. Thus, the fatigue reliability index of a structural member M_i, denoted β_{Mi}, can be computed by modelling the member as a subsystem of serially connected components. Thus, after [24], we get

$$\beta_{Mi} = -\Phi^{-1}(1 - \Phi(\boldsymbol{\beta}_{Ci}; \boldsymbol{\rho}_M)), \tag{8}$$

where $\Phi(\cdot)$ is the n_i-dimensional standard normal cumulative distribution function, $\boldsymbol{\beta}_{Ci}$ is the $1 \times n_i$ vector with all terms equal to β_{Ci} and $\boldsymbol{\rho}_M$ is the $n_i \times n_i$ correlation matrix, with ones in the diagonal and all non-diagonal terms equal to ρ_M.

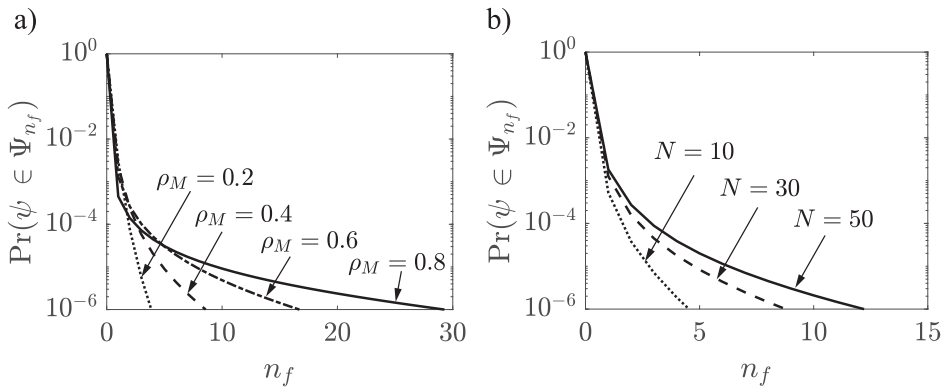

Fig. 5. Probability of occurrence of the deterioration states associated with n_f failed-members $\psi \in \Psi_{n_f}$ for the case of two equally reliable hot spots per member with fatigue reliability index $\beta_C = 4.0$. (a) For varying ρ_M and $N = 50$ members; (b) For varying system size N and $\rho_M = 0.5$.

By following this approach, we can now express the system as a combination of members that are subject to fatigue failure, which effectively behave as equivalent components. To build the joint deterioration model, we still need to compute the pair-wise correlation coefficient among members' safety margins, denoted $\rho'_{M,ij}$ $(i, j = 1, 2, \ldots, N)$. These correlation coefficients can be computed for each pair of members as a function of ρ_M, the reliability indices of the hot spots, and the number of hot spots in each member, as described in Appendix A. In general, each pair of members' fatigue safety margins will be associated with different correlations. According to [25], the average correlation coefficient can generally be used with satisfactory accuracy, leading to low error for parallel systems and being on the safe side for series systems. The average correlation coefficient, denoted ρ'_M, can be computed as

$$\rho'_M = \frac{2}{N(N-1)} \sum_{i=1}^{N} \sum_{j=1}^{i-1} \rho'_{M,ij}. \tag{9}$$

According to the findings in Appendix A, these correlation coefficients mainly depend on the correlation coefficient among components' safety margins ρ_M. Thus, if ρ_M is constant for all pairs of components, then the variability among all $\rho'_{M,ij}$ will be very small and the coefficient ρ'_M from Eq. (9) can be confidently used for all pairs of members' fatigue safety margins.

Let $\Psi_{n_f} \subset \Psi$ represent the subset of deterioration states associated with exactly n_f members failed due to fatigue. The probability that any particular n_f members are simultaneously failed in a system with N members, i.e., $\Pr(\psi)$ with $\psi \in \Psi_{n_f}$, is given by the following equation, after [26,24]:

$$\Pr(\psi) = \int_{-\infty}^{\infty} \varphi(u) \prod_{i=1}^{n_f} \Phi\left(\frac{u\sqrt{\rho'_M} - \beta_{Mi}}{\sqrt{1-\rho'_M}} \right) \prod_{i=n_f+1}^{N} \Phi\left(\frac{\beta_{Mi} - u\sqrt{\rho'_M}}{\sqrt{1-\rho'_M}} \right) \mathrm{d}u, \quad \text{with } \psi \in \Psi_{n_f}, \tag{10}$$

where $\varphi(\cdot)$ is the standard normal probability density function. It is assumed that the member reliability indices β_{Mi} (for $i = 1, 2, \ldots, N$) are ordered such that $i \in [1, n_f]$ are failed members and $i \in [n_f + 1, N]$ are non-failed members.

In Fig. 5, the probability $\Pr(\psi \in \Psi_{n_f})$, computed from Eq. (10) as a function of the number of failed members n_f, is shown for various values of the correlation coefficient ρ_M and of the number of deteriorating members N. See that the probability of occurrence of a given deterioration state increases with the number of members in the structure N and the correlation coefficient ρ_M, whereas it decreases with the number of failed members n_f.

2.3. Reliability of the deteriorating system

The annual probability of system failure at a given point in time, denoted $P_{f,sys}(t)$, can be computed applying Eq. (1). If the fatigue reliabilities of the hot spots are set to a certain value, the probability of occurrence of the deterioration states are independent of time, and consequently the annual probability of system failure can be denoted $\Pr(C)$ or $P_{f,sys}$. Eq. (1) requires to assess the system resistance for 2^N deterioration states, which becomes unreasonable, even for relatively small systems. A method to estimate upper and lower bounds of $P_{f,sys}$ within feasible computational time is proposed in the following section.

3. Truncation algorithm for system reliability bounds estimation

The goal is estimate the system reliability, as defined in Eq. (1), within feasible computational time. Typically, a large number of the possible deterioration states in Ψ are unlikely to realise, because they are associated with several members failed due to fatigue. Moreover, the ultimate capacity of the structure tends to be low or even zero for severe deterioration states. Thus, we propose to sequentially compute the conditional probabilities of system failure $\Pr\left(C|\psi_p\right)(p = 0, 1, \ldots, 2^N - 1)$ in Eq. (1) from less to more severe deterioration states. That is, the conditional probabilities are first calculated for the intact state ($\Psi = \psi_0$), then for all first-member-failure combinations (Ψ_1), and so on. Naturally, all the deterioration states would be taken into account after all the states in Ψ_N are computed. Although this would not be an approximation of Eq. (1), the sequential computation would in itself greatly reduce the number of evaluations for systems with low redundancy, according to the following theorem:

Theorem 1. *Let the mean ultimate resistance of the system conditional on a given deterioration state ψ be zero, i.e., $R_m(\psi) = 0$, $\psi \in \Psi_{n_f}$. Then, the mean ultimate resistance will also be zero for a deterioration state ψ' such that all the members that are failed in ψ are also failed in $\hat{\psi}$, i.e., $R_m(\hat{\psi}) = 0$ for any $\hat{\psi} \in \Psi_{n'_f}$, with $n'_f \geq n_f$.*

Proof. Structural deterioration is a time process. Thus, a deterioration state $\hat{\psi}$ consisting of n_f given members being failed cannot be realised before a state ψ with only $n_f - 1$ of those members being failed. Thus, if the structure is not able to bear any load for the deterioration state ψ, the system would remain failed after additional member failures. □

Furthermore, the following corollary can be deduced from Theorem 1:

Corollary 1.1. *Let $R_m(\psi) = 0$, $\forall \psi \in \Psi_{n_f}$. Then, $R_m(\hat{\psi}) = 0$, $\forall \hat{\psi} \in \Psi_{n'_f}$, such that $n'_f \geq n_f$.*

In other words, if the mean ultimate resistance is zero for all deterioration states associated with n_f failed-members, so it will be for any deterioration states with more than n_f failures. Thus, when the condition in Corollary 1.1 would be satisfied, one could avoid calculating more complex deterioration states, i.e., states with more failed members. However, this condition may not be met for small n_f for highly redundant systems. For those systems, the computation can be stopped after reaching a so-called truncation limit, denoted n_{lim}, i.e., after computing the conditional probabilities associated with deterioration states in $\Psi_{n_{lim}}$. Note that the estimation of the system reliability is exact when the condition in Corollary 1.1 is met for $n_f \leq n_{lim}$. The truncation limit should be sensibly chosen so that Eq. (1) can be estimated with sufficient accuracy. Based on the described sequential approach, upper and lower bounds, respectively denoted $P^{LB}_{f,sys}(t)$ and $P^{LB}_{f,sys}(t)$, can be estimated such that

$$P^{LB}_{f,sys}(t) \leq P_{f,sys}(t) \leq P^{UB}_{f,sys}(t). \tag{11}$$

First, we divide the set of possible deterioration states into two subsets $\Psi = \Psi^A \cup \Psi^B$. The subset $\Psi^A \subset \Psi$ contains all deterioration states with n_{lim} or less failed members, i.e., with $n_f \in [0, n_{lim}]$. The subset $\Psi^B \subset \Psi$ comprises all deterioration states with more than n_{lim} failed-members, i.e., with $n_f \in [n_{lim}+1, N]$. A lower bound can be found by setting the conditional probabilities of failure for all states $\psi \in \Psi^B$ equal to zero:

$$P^{LB}_{f,sys} = \sum_{\psi \in \Psi^A} \Pr(C|\psi) \Pr(\Psi = \psi). \tag{12}$$

Nevertheless, a better lower bound can be found by noting that the conditional probabilities of collapse associated with the deterioration states $\psi \in \Psi^B$ are, in average, at least as high as the failure probabilities associated with states with n_{lim} failures, which we denote $P^{n_{lim}}_{f,sys} = \mathbb{E}[\Pr(C|\psi \in \Psi_{n_f})]$ for simplicity. Therefore, a better lower bound is given by

$$P^{LB}_{f,sys} = \sum_{\psi \in \Psi^A} \Pr(C|\psi) \Pr(\Psi = \psi) + P^{n_{lim}}_{f,sys} \sum_{\psi \in \Psi^B} \Pr(\Psi = \psi). \tag{13}$$

The upper bound is given by assuming that $\Pr(C|\psi) = 1$ for all states in Ψ^B, that is:

$$P^{UB}_{f,sys} = \sum_{\psi \in \Psi^A} \Pr(C|\psi) \Pr(\Psi = \psi) + \sum_{\psi \in \Psi^B} \Pr(\Psi = \psi). \tag{14}$$

Note that the difference between the upper an lower bounds is given by

$$P^{UB}_{f,sys} - P^{LB}_{f,sys} = (1 - P^{n_{lim}}_{f,sys})(1 - \sum_{\psi \in \Psi^A} \Pr(\Psi = \psi)). \tag{15}$$

When sequentially computing the conditional probability of system failure, information about states with no resistance, i.e., $R_m(\psi) = 0$, can be used to reduce the number of assessed combinations. This is described in pseudo-code in Algorithm 1 in Appendix C. We introduce an n_f-dimensional matrix $\mathbf{A}_{[n_f]}$ called the event matrix. Each term of $\mathbf{A}_{[n_f]}$ refers to the conditional probability of system failure associated with a specific combination of n_f failed-members. For example, $\mathbf{A}_{[2]}(i,j)$ contains the system failure probability conditioned on members i and j being failed. If any combination with the failed members i and j has a failure probability of one, the same will be true for all other combinations including these failures. The sequential assessment of the terms of the event matrices is presented in pseudo-code in Algorithm 2, see Appendix C.

4. Validation of the HSE and EDS design methods

In this section, we address the methodology for assessing the validity of the HSE and the EDS design methods. For a given system and a given annual target reliability index β^T_{sys}, these methods can be used to estimate the required fatigue reliabilities of the hot spots. In general, the system reliabilities associated with the obtained fatigue designs will differ from the target value, because the design methods are based on simplifications. One can estimate the bounds of the associated system reliabilities by applying the truncation algorithm described in the previous section. In the present investigation, we apply this approach to the considered bracing systems (see Fig. 2) to study the inherent safety level of these design methods for typical jacket configurations.

As previously mentioned, the HSE design method consists in finding the hot-spots' fatigue reliabilities that lead to an equal contribution of the members to the target system reliability based on the HSE approximation shown in Eq. (2). As already discussed, the HSE approximation is valid for independent fatigue safety margins and for systems with low redundancy. Hence, the members' design reliabilities, denoted $\beta_{Mi,d}$ (with $i = 1, \ldots, N$), are obtained according to the following equation:

$$\beta_{Mi,d} = -\Phi^{-1}\left(\frac{\Phi(-\beta^T_{sys}) - \Phi(-\beta_{sys,0})}{N \cdot \Pr(C|\psi_i)}\right), \text{ with } i = 1, \ldots, N; \tag{16}$$

where $\psi_i = \{\bar{F}_1 \cap \cdots \cap \bar{F}_{i-1} \cap F_i \cap \bar{F}_{i+1} \cap \cdots \cap \bar{F}_N\}$. Eq. (16) is only defined when $\Phi(-\beta^T_{sys}) - \Phi(-\beta_{sys,0}) \leq N \cdot \Pr(C|\psi_i)$. The members for which this condition is not met can be interpreted to be of so little importance that they do not need to be designed for fatigue according to this method.

The EDS method overcomes some of the limitations associated with the HSE method. In the EDS method, the contributions of the different hot spots of the system are modelled with separate EDS models. An EDS model is an idealised system consisting of several Daniels systems in series. Daniels systems are well studied purely parallel systems [27,28]. The EDS models have two parameters, namely the number of elements in each Daniels system and the number of Daniels systems in series. The first parameter is calibrated so that the conditional probability of failure of the EDS given failure of one of the Daniels element is equal to the conditional failure probability of the true system given failure of the hot spot of interest. Therefore, this parameter is a measure of the redundancy of the system with respect to failure of the regarded hot spot. Moreover, this parameter contains information about the probabilistic load and resistance models of the true system. The second parameter is common to all the EDS models that represent a given system, and is found such that it characterises the number of deteriorating hot spots of the actual system. More information about the EDS method and how to compute the parameters of the EDS models can be found in [5].

Compared to the HSE method, the EDS method enhances fatigue design by explicitly taking the dependence among fatigue processes into account. Moreover, the redundancy of a system is partially captured through the EDS models. Note that the redundancy of the system is still characterised only by first-member-failure deterioration states. Thus, more complex deterioration states are only approximated by the behaviour of the calibrated EDS models.

As a reference, the associated computational times associated with the bracing system BC2 are reported based on the described FE models in USFOS and using a processor Intel(R) Xeon(R) CPU E5520 @ 2.27 GHz 2.26 GHz (2 processors). The assessment of the ultimate capacity conditional on a deterioration state takes in average approx. 7 s. Thus, the assessment of all $N + 1 = 49$ deterioration states that need to be assessed takes $7 \cdot 49 = 343$ s. The assessment of the HSE and EDS methods requires 0.01 s and 0.24 s respectively, provided that the required inputs are pre-computed. Thus, the computational demands of the two considered design methods are practically the same, as the costs are driven by the assessment of the FE models and both methods need assessing the same number of FE models.

5. Results

5.1. Convergence of the truncation algorithm

One of the benefits of the proposed truncation algorithm is the reduction of deterioration states to be computed, due to the possibility of deducing which states are associated with certain failure from the

Table 1
Number of conducted pushover analyses/total number of distinct deterioration states, for states ordered according to the number of simultaneously failed members n_f and shown for the considered bracing systems BC1, BC2, BC3.

n_f	BC1	BC2	BC3
0	1/1	1/1	1/1
1	36/36	48/48	36/36
2	435/630	1128/1128	406/630
3	2353/7140	16853/17296	1383/7140
4	5951/58905	183093/194580	2138/58905

computations in the previous step. This reduction is shown in Table 1 for the considered bracing systems by comparing the computed pushover analyses with the total number of deterioration states. The total number of deterioration states for given n_f can be computed from combinatorics as $\frac{N!}{n_f!(N-n_f)!}$. It can be deduced from Table 1 that the conditional probability of system failure is equal to one for 87%, 1% and 94% of the cases for BC1, BC2 and BC3, respectively, by taking all the states associated with up to 4 failed-members into account. Higher reductions are achieved for less redundant systems, for which a larger number of highly deteriorated states will predictably be associated with no bearing capacity. Thus, BC3 is the less redundant system of the three. In contrast, BC2 is a highly redundant system and almost no reduction of cases is obtained. Additionally, it can be seen that the larger n_f, the larger the achieved reduction, as it could be expected. The computational costs of assessing the bounds of the probability of failure with a truncation limit $n_{lim} = 4$ are also reported here as a reference. These computations took approximately 16 h, 223 h and 7 h, for BC1, BC2 and BC3, respectively, by using a processor Intel(R) Xeon(R) CPU E5520 @ 2.27 GHz 2.26 GHz (2 processors).

The truncation algorithm provides the upper and lower bounds of the system probability of failure as an outcome, which are determined in accordance with Eqs. (13) and (14). Fig. 6 shows the convergence of the upper and lower bounds towards the exact value for increasing truncation limit n_{lim}. For illustration purposes, we consider all the hot spots to have a fatigue reliability index $\beta_C = 4$, all the fatigue limit states to be correlated with coefficient $\rho_M = 0.7$, and all the members to contain two hot spots ($n = 2$). The maximum considered truncation limit is $n_{lim} = 4$ due to computational limitations. It can be seen that the bounds provide a relatively narrow band to estimate the system reliability for the less redundant bracing systems BC1 and BC3. Furthermore, the HSE approximation provides a rather accurate estimation for these two systems. In contrast, the estimation band is broader for BC2, suggesting that deterioration states with more than four failed-members cannot be neglected in order to accurately estimate the system reliability for this system. Moreover, the HSE approximation yields a large overestimation of the system reliability index in this case. This observation is in line with the results by Straub and Der Kiureghian [5], which shows that the HSE approximation fails for systems with significant redundancy and large correlation coefficient ρ_M.

The contributions of the subsets Ψ_{n_f} (with $n_f = 1, 2, \ldots, 4$) to the probability of system failure are plotted in Fig. 7. The contributions are computed relative to the upper bound of the probability of system failure. Moreover, the authors show the contribution of the deterioration states with more than 4 failed-members, highlighted in lighter colour. The contribution of these states is unknown since the truncation limit is set to $n_{lim} = 4$. However, we know that it will be somewhere between near zero and the plotted contribution, which corresponds to the difference between the upper and lower bounds as given by Eq. (15). It can be seen that the assumption in [9] suggesting that deterioration states with more than one failed member do not significantly contribute to the system probability of failure does not hold for typical jacket configurations.

Table 2
Calibrated members' reliability indices for a target annual system reliability index $\beta^T_{sys} = 3.7$ using the HSE design method. Mean values are shown for the leg, diagonal and horizontal groups.

	BC1	BC2	BC3
Legs	2.82	1.00[a]	2.34
Diagonals	1.35	1.00[a]	1.87
Horizontals	1.04	1.00[a]	–

[a]A minimum member reliability index $\beta_M = 1.00$ is imposed.

Table 3
Calibrated members' reliability indices for a target annual system reliability index $\beta^T_{sys} = 3.7$ using the EDS design method. Mean values are shown for the leg, diagonal and horizontal groups. Results are given for two values of the correlation coefficient among members' fatigue safety margins ρ'_M.

	BC1		BC2		BC3	
	$\rho'_M = 0.0$	$\rho'_M = 0.7$	$\rho'_M = 0.0$	$\rho'_M = 0.7$	$\rho'_M = 0.0$	$\rho'_M = 0.7$
Legs	3.91	3.96	3.18	4.01	3.23	3.37
Diagonals	3.11	3.24	3.19	4.01	3.47	3.57
Horizontals	2.86	3.01	3.12	4.00	–	–

5.2. System effects

In this section, we study numerically how the predictions of the upper and lower bounds and the HSE approximation are affected by system effects. The effects of the component reliability index β_C and of the correlation coefficient among the hot spots safety margins ρ_M are shown in Figs. 8 and 9. The figures show the upper and lower bounds of the system reliability index β_{sys}, as well as the HSE approximation computed using Eq. (2). Generally, it can be seen that the distance between the lower and the upper bounds decreases with β_C and increases with ρ_M, being practically negligible for $\rho_M \leq 0.3$. A similar pattern can also be appreciated regarding the accuracy of the HSE approximation. For BC2, however, higher component reliabilities should be specified for the HSE approximation to provide accurate predictions for low values of ρ_M. It is concluded that having uncorrelated fatigue limit states is not always enough for the HSE approximation to provide accurate predictions.

The trends observed in Fig. 9 indicate that BC1 and BC3 largely behave as series systems, since their system reliability indices remain practically constant for correlations in the range $0 \leq \rho_M \leq 0.6$ and drastically increase for high correlation values. On the contrary, the more redundant system BC2 behaves closer to a parallel system, with the system reliability index decreasing in the range $0 \leq \rho_M \leq 0.8$, and increasing afterwards.

5.3. Inherent safety of the HSE and EDS design methods

The inherent safety of the HSE and EDS design methods is assessed according to the methodology presented in Section 4. The HSE and EDS methods are applied to the fatigue design of the three considered bracing systems (see Fig. 2). The required fatigue reliability are calibrated using a target annual system reliability index $\beta^T_{sys} = 3.7$ for BC1, BC2 and BC3. The obtained results are summarised in Tables 2 and 3, distinguishing between leg, diagonal and horizontal members. Note that the results of the HSE method are not shown for varying ρ'_M, since they do not depend on this parameter. It can be seen that the values calibrated with the HSE design method are considerably lower than those obtained with the EDS method.

The obtained design fatigue reliability indices for the jacket BC1 are plotted in Fig. 10 as a function of the residual influence factor RIF, which is a common measure of the redundancy of a system with respect to first-member-failure deterioration states [29–31]. The RIF

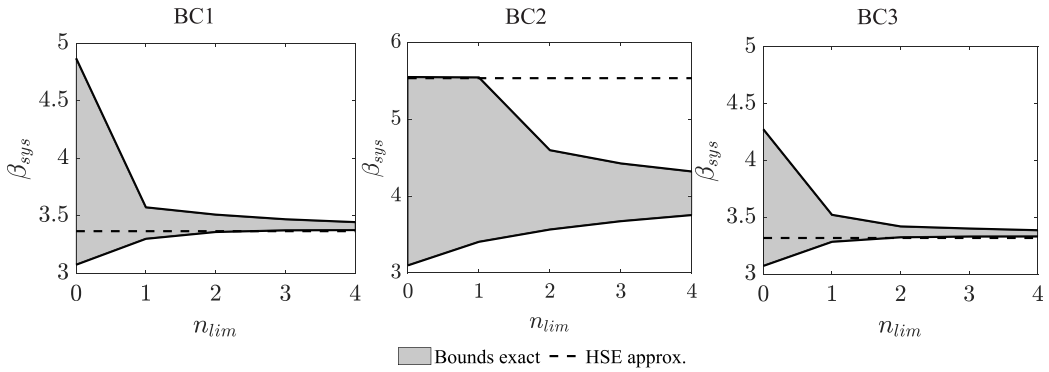

Fig. 6. Convergence of the estimation of the system reliability index β_{sys} by means of the truncation algorithm for increasing truncation limit n_{lim}, for the considered jacket systems BC1, BC2 and BC3. Results are compared with the HSE approximation in Eq. (2). Inputs: $\beta_C = 4$, $\rho_M = 0.7$, and $n = 2$.

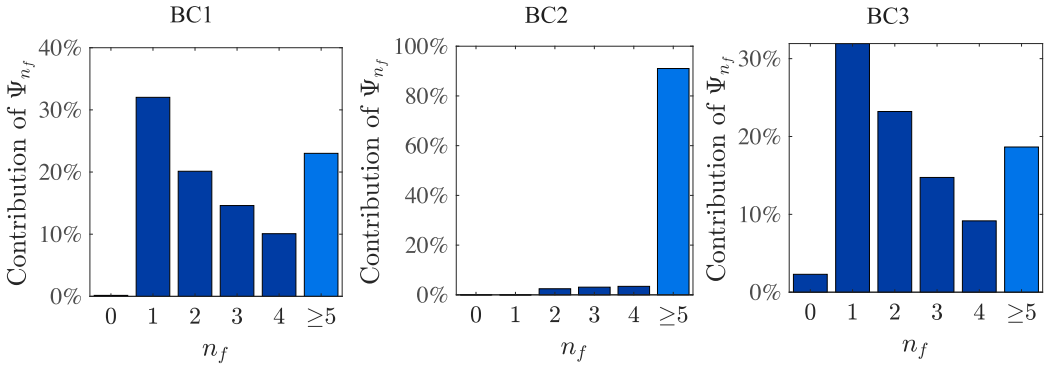

Fig. 7. Contribution to the probability of system failure of the deterioration states in the subsets Ψ_{n_f} ($n_f = 1, 2, \ldots, 4$), plus those with $n_f \geq 5$. The contribution of the deterioration cases with more than 4 failed-members is shown in lighter colour, to highlight that this contribution is uncertain. Inputs: $n_{lim} = 4$, $\beta_C = 4$, $\rho_M = 0.7$, and $n = 2$.

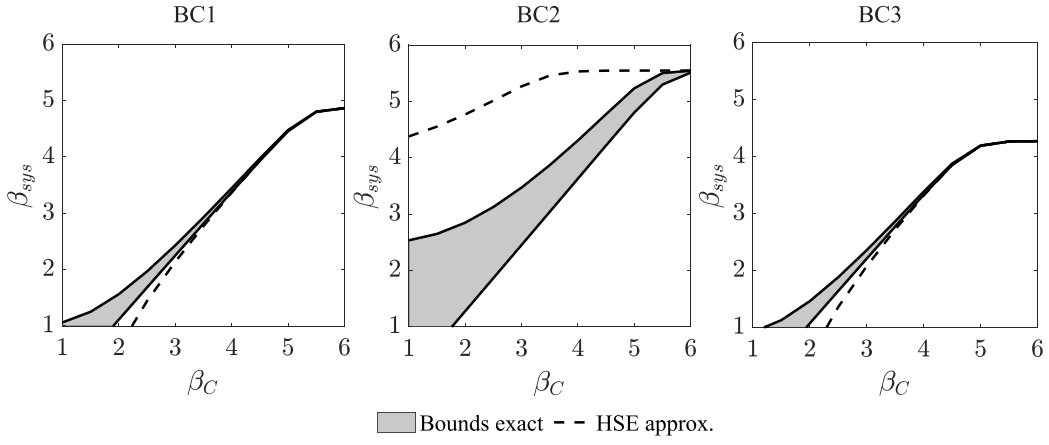

Fig. 8. System reliability index as a function of the component reliability β_C. Results are compared with the HSE approximation in Eq. (2). Inputs: $\rho_M = 0.7$; $n_{lim} = 4$.

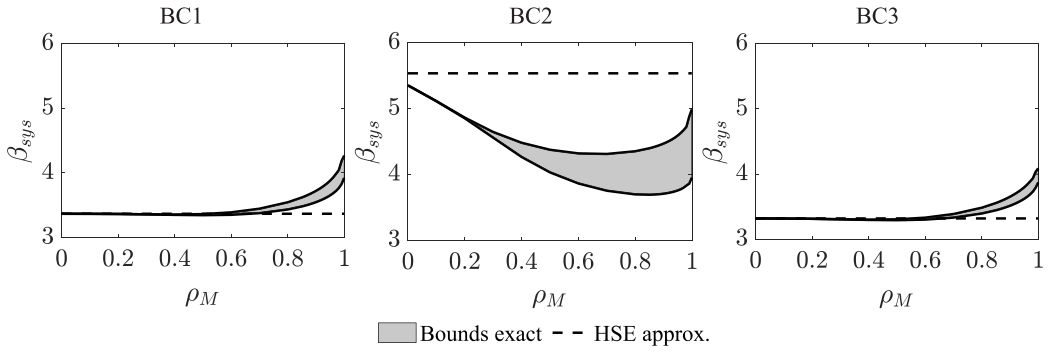

Fig. 9. System reliability index as a function of the correlation coefficient ρ_M. Results are compared with the HSE approximation in Eq. (2). Inputs: $\beta_C = 4$, $n_{lim} = 4$.

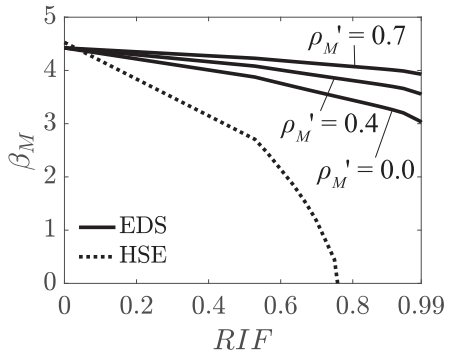

Fig. 10. Calibrated members' reliability indices of the bracing system BC1 as a function of the residual influence factor RIF. Results are associated with a target annual system reliability index $\beta_{sys}^{T} = 3.7$. The results of the EDS method are shown for various values of the pair-wise correlation coefficient among members' safety margins ρ_M'.

of a system with respect to failure of a member i, denoted RIF_i, is defined as:

$$RIF_i = \frac{R_{m,F_i}}{R_{m,0}}, \tag{17}$$

where $R_{m,0}$ is the mean ultimate resistance of the intact structure and R_{m,F_i} is mean the ultimate resistance given failure of member i. The RIF of the different member types are shown in Table B.6 in Appendix B for the three bracing systems. Fig. 10 shows that the HSE method tends to underestimate the required members' reliabilities for increasing RIF.

The calibrated members reliability indices with both design methods are then used in the estimation of the associated upper and lower bounds of the annual system reliability index β_{sys}. The results are shown in Fig. 11 as a function of ρ_M'. It can be seen that the reliability level associated with the EDS method is closed to the target value, whereas the HSE method consistently leads to insufficient reliability.

6. Discussion

The results in Figs. 8 and 9 show that the HSE approximation provides accurate estimations of the system reliability for low values of the correlation coefficient among fatigue safety margins when the system reliability is high. Nevertheless, for the three tested bracing systems, the reliabilities of the designs obtained following the HSE method were significantly lower than the target value, as shown in Fig. 11. The computed low system reliabilities are explained by the fact that the HSE method leads to an under-design of non-critical members, as shown in Fig. 10. Non-critical members are associated with high RIF values, or equivalently, with low probabilities of structural collapse given failure of these members. Despite these members being non-critical when it comes to first-failure deterioration states, they may be more important for deterioration states with several simultaneously failed members. Therefore, they may potentially contribute to the system probability of failure in a significant manner. Based on these results, the authors do not recommend to use the HSE design method for jacket-type systems, as it may lead to insufficient system reliability.

The EDS design method provides significant improvements with respect to the HSE method. The reliability associated with the designs obtained based on this method are close to the target value for the considered bracing systems, as shown in Fig. 11. Nevertheless, it is not guaranteed that the fatigue designs will satisfy the target level. A solution to this issue is to use the truncation algorithm to verify the safety level of the obtained design and to guide the design reassessment if necessary.

Regarding the computational efficiency of the truncation algorithm, the authors showed that narrow bands for the system reliability can be estimated within feasible computational time. The number of global pushover analyses to be computed is a function of the truncation limit n_{lim}, which should be chosen dependent on the redundancy of the system. For highly redundant systems with many members, the number of analyses to be computed may be large. Nevertheless, the assessment of the pushover analyses is highly parallelizable, due to the uncoupling between the fatigue and ultimate load limit states in Eq. (1). Further research could be devoted to improving the computational efficiency of the proposed methodology. Moreover, the authors suggest to further study the possibility of finding better approximate solutions to Eq. (1) by considering the tendency of the upper and lower bounds as a function of the truncation limit shown in Fig. 6.

Generally, the determination of the probability of failure of a deteriorating system requires solving a time-variant reliability problem. As indicated in Section 1.1, the solution of Eq. (1) leads to the so-called interval annual probability of system failure during an arbitrary year $(t-1, t]$, as defined by Straub et al. [6]. To account for the fact that the system may have failed during any of the previous years, one needs to assess the cumulative probability of failure. The cumulative probability of failure at year t is the probability of the union of the annual failure events up to year t, which can be assessed, based on the bounds for series systems [32], using the time-interval probabilities of failure obtained from Eq. (1) from years 0 to t [6]. Therefore, the present research is a step forward in the process of assessing the time-variant reliability of fatigue-deteriorating lattice structures. Further studies should be conducted to assess bounds of the cumulative probability of system failure based on the bounds in Eqs. (13) and (14).

7. Conclusions

A novel approach, called the truncation algorithm, for assessing the system reliability of offshore lattice structures subject to extreme environmental loading and fatigue was proposed in this article. The truncation algorithm allows to estimate a narrow band of the probability of system failure within feasible computational time when applied to fatigue designs with high annual system reliability. The truncation algorithm was used to assess the performance of two existing fatigue design methods, here called the HSE and EDS methods. The results of the study showed that the HSE method highly overestimates the system reliability for redundant systems and leads to designs with insufficient system reliability for common jacket configurations. In contrast, the EDS method leads to significantly better designs, with near-target reliabilities irrespective of the statistical dependence among fatigue limit states and the level of redundancy of the system. Because the HSE and EDS methods have comparable computational times, the EDS is a more attractive method. The proposed truncation algorithm comes with longer, but still feasible computational time. Due to the higher computation times, it is not efficient to apply the truncation algorithm for reliability-based design. Nonetheless, it can be used to verify that the reliability of the designs obtained with the EDS method is sufficient. Furthermore, the results of the study showed that, contrary to previous expectations, complex deterioration states with several members failed due to fatigue significantly contribute to the probability of system failure for common jacket bracings. Consequently, non-critical members should not be designed only taking into account first-member-failure deterioration states.

Appendix A. Correlation among members' safety margins

We consider a system with two members M_1 and M_2, each containing n equally reliable hot spots. Let the hot spots of M_1 and M_2 be associated with reliability indices β_{C1} and β_{C2}, respectively. Moreover, let the hot spots be statistically dependent with pair-wise correlation coefficient among the hot-spots' safety margins ρ_M. The objective is to compute the correlation coefficient among members' safety margins

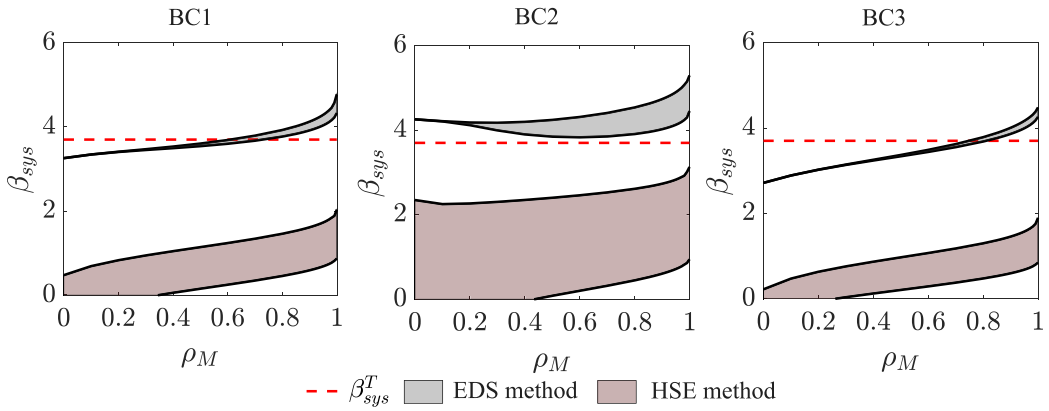

Fig. 11. Inherent safety level of the EDS and HSE design methods, illustrated by the upper and lower bounds of the annual system reliability index β_{sys}. The employed members' reliability indices are calibrated to an annual target reliability index $\beta_{sys}^T = 3.7$.

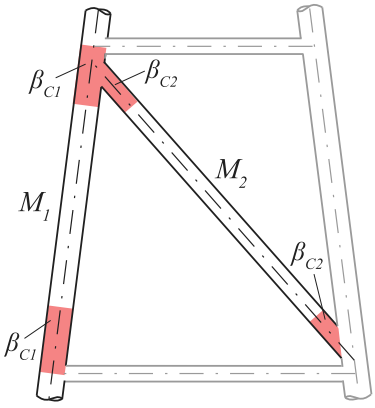

Fig. A.12. Subsystem conformed by members M_1 and M_2, each containing two hot spots (coloured in red). The hot spots of M_1 and M_2 are associated with reliability indices β_{C1} and β_{C2}, respectively.

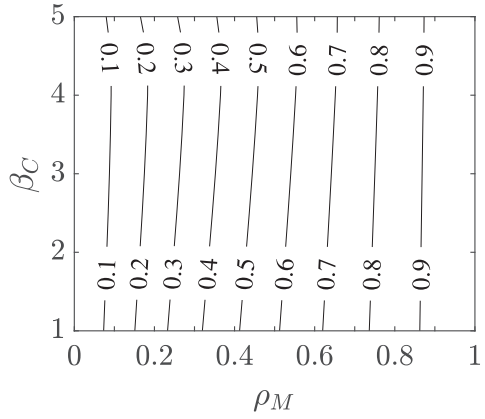

Fig. A.13. Contours correspond to the correlation coefficient among members' safety margins ρ'_M as a function of the hot-spot reliability index β_C and correlation coefficient among components' safety margins ρ_M for the case of two hot spots per member.

ρ'_M. A system such as the subsystem formed by M_1 and M_2 in Fig. A.12 meets these premises.

The binary condition of the hot spots E_i ($i \in [1, 2n]$) are Bernoulli distributed random variables, with parameters $p_{fc1} = \Phi(-\beta_{C1})$ and $p_{fc2} = \Phi(-\beta_{C2})$ for the hot spots of M_1 and M_2, respectively. Note that failure and survival of the hot spots are represented by the Bernoulli variables taking the values 1 and 0, respectively. Moreover, the binary condition of the members E'_1 and E'_2 are also Bernoulli distributed, with parameters $p_{fm1} = \Phi(-\beta_{M1})$ and $p_{fm2} = \Phi(-\beta_{M2})$, respectively. The reliability indices β_{M1} and β_{M2} can be computed according to Eq. (8) given β_{C1}, β_{C2} and ρ_M.

The probability of the joint event $\{E'_1 = 0, E'_2 = 0\}$, i.e., $\Pr(E'_1 = 0, E'_2 = 0)$, can be expressed as a function of ρ'_M using Eq. (8), by noting that this probability is the opposite of the probability of failure of a system with two serially connected members, i.e.,:

$$\Pr(E'_1 = 0, E'_2 = 0) = 1 - \Pr(E'_1 = 1 \cup E'_2 = 1) = \boldsymbol{\Phi}(\boldsymbol{\beta}_M; \boldsymbol{\rho}'_M), \tag{A.1}$$

where $\boldsymbol{\beta}_M = [\beta_{M1}, \beta_{M2}]$ and $\boldsymbol{\rho}'_M$ is the 2×2 correlation matrix with all non-diagonal terms equal to ρ'_M.

Moreover, this probability can be computed from the joint probability function of the components' conditions applying Eq. (10):

$$\Pr(E'_1 = 0, E'_2 = 0) = \int_{-\infty}^{\infty} \varphi(u) \left[\Phi\left(\frac{\beta_{C1} - u\sqrt{\rho_M}}{\sqrt{1-\rho_M}}\right)\right]^n \left[\Phi\left(\frac{\beta_{C2} - u\sqrt{\rho_M}}{\sqrt{1-\rho_M}}\right)\right]^n \mathrm{d}u. \tag{A.2}$$

By substituting Eq. (A.1) in (A.2), we obtain the following equality from which ρ'_M can be numerically computed:

$$\boldsymbol{\Phi}(\boldsymbol{\beta}_M; \boldsymbol{\rho}'_M) = \int_{-\infty}^{\infty} \varphi(u) \left[\Phi\left(\frac{\beta_{C1} - u\sqrt{\rho_M}}{\sqrt{1-\rho_M}}\right)\right]^n \left[\Phi\left(\frac{\beta_{C2} - u\sqrt{\rho_M}}{\sqrt{1-\rho_M}}\right)\right]^n \mathrm{d}u. \tag{A.3}$$

The correlation coefficient ρ'_M is plotted as a function of β_C and ρ_M in Fig. A.13 for member's containing two hot spots each, all with reliability index β_C.

Lastly, the correlation coefficient among the components' failure events is computed to illustrate the difference between the two. For this purpose, we consider the particular case of two members, each containing two hot spots with reliability index β_C. The binary condition of any of the components is then $E_i \sim Be(p_{fc})$, with $p_{fc} = \Phi(-\beta_C)$ and $i = [1, 4]$. The probability of the joint event of any two components surviving ($\{E_i = 0, E_j = 0\}$ with $i \neq j$) is given by

$$\Pr(E_i = 0, E_j = 0) = (1 - p_{fc})^2 + \mathrm{COV}[E_i, E_j] \quad \text{for } i \neq j, \tag{A.4}$$

by definition of the Bernoulli variables; where $\mathrm{COV}[E_i, E_j]$ is the covariance between E_i and E_j, which for Bernoulli variables is given by

$$\mathrm{COV}[E_i, E_j] = \rho_E \cdot p_{fc}(1 - p_{fc}) \quad \text{for } i \neq j, \tag{A.5}$$

with ρ_E being the correlation coefficient among component's failures. Plugging the relation in Eq. (A.5) into Eq. (A.4) and isolating the

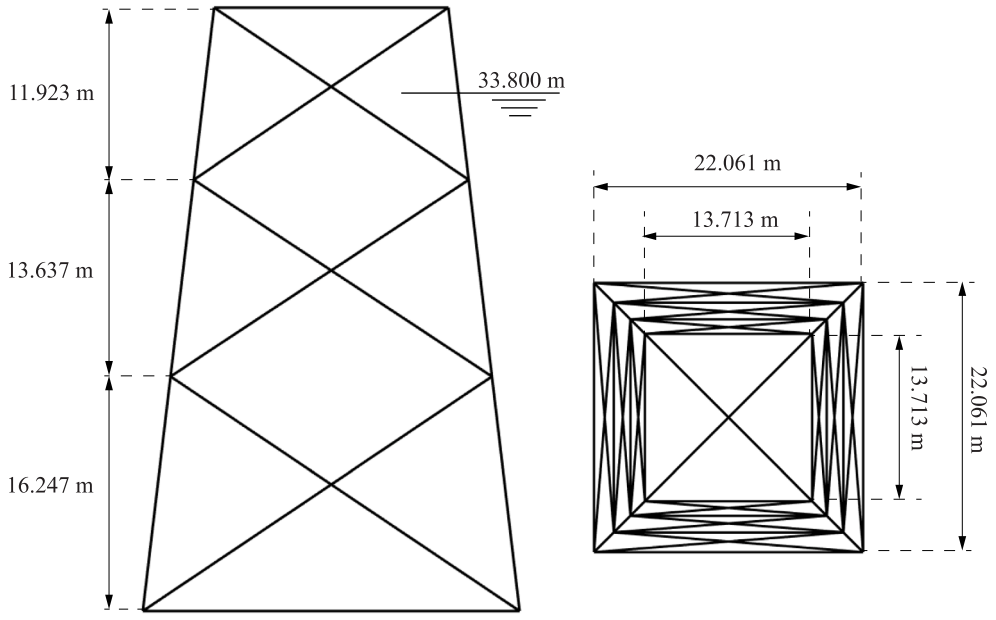

Fig. B.14. Main dimensions of the studied lattice structures.

Table B.4
Environmental input associated with the 100 year wave load.

Variable	Value
Water depth at HAT, h_w	33.8 m
Significant wave height, $H_{s,100}$	16 m
Peak period, T_z	12 s
Associated current velocity u_c	2.2 m/s
Current blockage factor, a_{cb}	0.8
Wave spread factor, a_{wk}	0.9
Drag coefficient, C_d	0.75
Inertia coefficient, C_m	2
Marine growth	70 mm

Note: HAT = Highest astronomical tide.

correlation coefficient ρ_E leads to

$$\rho_E = \frac{\Pr(E_i = 0, E_j = 0) - (1 - p_{fc})^2}{(1 - p_{fc})p_{fc}}, \quad \text{for } i \neq j. \tag{A.6}$$

Applying Eq. (A.6) with component reliability index $\beta_C = 3$, i.e., $p_{fc} = 0.0013$, and pair-wise correlation among safety margins $\rho_M = 0.5$ results in a correlation coefficient among failures $\rho_E = 0.059$, which is much smaller than $\rho_M = 0.5$.

Appendix B. ULS design of the jackets

The sea-state input for the environmental loads is shown in Table B.4. The three considered bracing systems are build based on the common dimensions shown in Fig. B.14. The structures are tower-type lattice systems, i.e., the piles are driven through guides around the legs at the base of the structure.

B.1. Nominal cross-section design

The design of the nominal cross-sections of the members is performed according to ULS as specified by ISO 19902:2007 [19]. In this standard, safety is assessed by means of a component-based partial safety factor format (PSFF) verification. The verification consists of ensuring that the factored stresses induced by the 100 year environmental load combined with the permanent loads are below the factored nominal capacities of the members. The capacity of the members is evaluated for combined axial and bending loads, including local buckling. The nominal yield strength of steel is taken as $F_{y,k} = 345$ MPa for all members.

Here, the design of the members is conducted iteratively by increasing the cross-section dimensions until the PSFF verification is satisfied. Although this approach does not lead to fully optimised designs, the results are considered sufficient for the purpose of the investigation. Diameters and thicknesses are increased in steps of 0.0508 m (2 inches) and 0.0032 m (0.125 inches), respectively. For the legs, thicknesses are increased unless the diameter over thickness ratio is larger than 50, in which case the diameter is increased. The same logic is followed for the bracing, in which case a diameter over thickness ratio of 25 is used.

The structural response is computed in each iteration step. Thus, a compromise between model sophistication and computational time is needed. Wave kinematics are computed according to Airy first order wave theory, including Wheeler stretching [33]. More complex wave kinematics and wave load models could be applied, including breaking and slamming loads, but the general conclusions in this paper are not expected to be highly influenced by such more complex loading models. The hydrodynamic loading is computed using Morison equation [34] on an equivalent stick model [20]. Resultant horizontal forces are integrated from the hydrodynamic load profile and applied at the leg nodes, i.e., at the intersection between the legs and the bracing system. The sum of all horizontal loading leads to the 100 year base shear E_{100}. The permanent loading results from the gravity and buoyancy forces of the members together with a top mass of 1600 t that is assumed to be equally distributed among the four legs. For the computation of the buoyancy, the legs are assumed to be flooded and the bracings are assumed to be either dry or flooded, taking the most severe of the two possibilities. To compute the axial forces of the members, the structure is assumed to behave as a truss system with pinned boundary conditions at the leg–soil interface. In addition to the axial loading, bending loads due to permanent and extreme environmental loads are computed assuming that the members are pinned at the connections. The accuracy of the models employed for this task is assumed to be sufficient for the current investigation. Particularly, because the same model assumptions are used for all tested bracing systems. Thus, any bias resulting from the assumptions similarly affects all results and will not likely disturb the drawn conclusions. Furthermore, a more sophisticated analysis is conducted to assess the ultimate mean resistance of

Table B.5
Global resistance and annual reliability index of the intact system for the 100 year environmental load.

	$R_{m,0}$ [MN]	RSR [–]	$\beta_{sys,0}$
BC1	11.98	2.46	4.87
BC2	21.57	3.12	5.55
BC3	12.31	2.00	4.27

Table B.6
Average residual influence factor RIF of the legs, diagonals and horizontals for the three bracing systems.

	BC1	BC2	BC3
Legs	0.43	0.94	0.65
Diagonals	0.81	0.92	0.71
Horizontals	0.93	0.97	–

the structure (see Appendix B.2), which is the magnitude used to assess the structural reliability of the system.

The jackets are designed at a fictitious location in the northern North Sea. The 100 year sea state input at this location is shown in Table B.4. The sea state is determined by the water depth h_w at the highest astronomical tide (HAT), the 100 year return period significant wave height $H_{s,100}$, and the associated peak period T_z and current velocity u_c. The current velocity is assumed constant in depth. Note that the top horizontal bars are 8 m above the HAT sea level. It is assumed that the current velocity is constant for all water depths. Moreover, to assess the hydrodynamic loading, we assume values for the marine growth and for the drag and inertia coefficients, denoted C_d and C_m, respectively. These values are taken constant for all members and water depths.

B.2. Global structural analysis

Firstly, the assessment of the global resistance of the structure against extreme environmental loading is presented. This assessment is based on non-linear pushover analysis for the intact and deteriorated systems. Secondly, the computation of the system reliability conditional on the deterioration states is elaborated on.

B.2.1. Pushover analysis

The mean structural capacity R_m is computed by means of a pushover analysis. The analysis is performed using the finite element analysis (FEA) software USFOS [35]. The hydrodynamic loading is assessed using Stokes 5th order theory. The mean values of the material properties are used in this analysis. The mean yield strength F_y is specified as 10% larger than the nominal yield strength $F_{y,k}$, in accordance with [21,19]. The model includes non-linear material behaviour, global buckling of the members, large displacements and deformations, formation of plastic hinges and load redistribution.

Initially, the unfactored permanent loads and the 100 year hydrodynamic loads are applied. After that, the 100 year hydrodynamic load profile is scaled up until global failure is reached. The analysis is stopped when one of the following two conditions is met: (a) the base-shear decreases to half of the maximal achieved base shear; or (b) the global displacement reaches 0.5 m. It is noted that condition (a) is reached first in the great majority of cases. After completion of the analysis, the mean ultimate base shear R_m is determined as the maximal computed base shear. The described analysis can be conducted for any given deterioration state $\Psi = \psi$, obtaining the mean ultimate resistance conditional on the deterioration state, denoted $R_m(\psi)$. The ultimate resistance of the intact system is denoted $R_{m,0}$.

The results of the global analysis of the intact structural systems are shown in Table B.5. The average RIF of the members, computed according to Eq. (17), are shown in Table B.6.

Note that the 100 year base shear is first computed according to Airy theory to assess the nominal cross-section design. After that, the global analysis is conducted based on a non-linear FE model that uses Stokes 5th order theory to assess the ultimate base shear. The two estimates of the 100 year base shears are presented in Table B.7, where they are denoted E^A_{100} and E^S_{100}, respectively. It is seen that the simplified hydrodynamic model used for ULS design provides relatively similar results than the more sophisticated one.

Table B.7
Comparison of the 100 year base shear computed with Airy theory on equivalent stick structure E^A_{100} and with Stokes 5th order theory E^S_{100}.

	E^A_{100} [MPa]	E^S_{100} [MPa]	Relative error
BC1	5.36	4.86	10.2%
BC2	6.05	6.92	12.5%
BC3	4.47	6.14	27.3%

Appendix C. Pseudo-codes for the truncation algorithm

The proposed truncation algorithm is presented in pseudo-code in Algorithms 1 and 2. In the proposed algorithm, pushover analyses are sequentially conducted from deterioration states with less to more simultaneously failed members. The results at the different steps of the algorithm are stored in the event matrices $\mathbf{A}_{[n_f]}$ $(n_f = 1, 2, \ldots, n_{lim})$.

Algorithm 1: Expansion of event matrix between two iterations

Function `ExpandEventMatrix`$(\boldsymbol{A}_{[n_f]})$**:**
  $\mathbf{A}_{[n_f+1]} = \mathbf{0}_{[n_f+1]}$;
  Apply knowledge of $\mathbf{A}_{[n_f]}$ to $\mathbf{A}_{[n_f+1]}$;
  E.g., for $n_f = 2$;
  for $i = 1, 2, ..., N$ **do**
    $\mathbf{A}_{[n_f+1]}(i,k,i) = \mathbf{A}_{[n_f]}(i,k), k = 1, 2, ..., N$;
    $\mathbf{A}_{[n_f+1]}(k,i,i) = \mathbf{A}_{[n_f]}(i,k), k = 1, 2, ..., N$;
    $\mathbf{A}_{[n_f+1]}(i,i,k) = \mathbf{A}_{[n_f]}(i,k), k = 1, 2, ..., N$;
  end
  for $i, j = 1, 2, ..., N$ **do**
    if $\boldsymbol{A}_{[n_f]}(i,j) = 1$ **then**
      $\mathbf{A}_{[n_f+1]}(i,j,k) = 1, k = 1, 2, ..., N$;
      $\mathbf{A}_{[n_f+1]}(i,k,j) = 1, k = 1, 2, ..., N$;
      $\mathbf{A}_{[n_f+1]}(k,i,j) = 1, k = 1, 2, ..., N$;
    end
  end
  return $\mathbf{A}_{[n_f+1]}$ with known information from $\mathbf{A}_{[n_f]}$;

Algorithm 2: Truncated sequential analysis of deterioration states

input : Truncation limit n_{lim}
output: $\Pr(C|\psi_p)\ \forall p \in \mathbb{N} : N_f(\psi_p) \geq n_f$
$n_f \leftarrow 0$;
$\mathbf{A}_{[n_f]} \leftarrow \mathbf{0}_{1\times N}$;
while $n_f \leq n_{lim}$ **do**
  Collect into $\hat{\Psi}_{n_f}$ the subset of deterioration states in Ψ_{n_f} for which the condition probability of failure is yet unknown:
  $\hat{\Psi}_{n_f} \leftarrow \psi \in \Psi_{n_f} : \mathbf{A}_{[n_f]} = 0$, with $\hat{\Psi}_{n_f} \subset \Psi_{n_f}$;
  Compute $R_m(\psi), \forall \psi \in \hat{\Psi}_{n_f}$ with pushover analysis;
  Compute $\beta_{sys}(\psi), \forall \psi \in \hat{\Psi}_{n_f}$ for $R_m(\hat{\Psi}_{n_f})$ using Eq. (6);
  Compute the conditional probabilities of system failure $\Pr(C|\psi) \leftarrow \Phi(-\beta_{sys}(\psi)), \forall \psi \in \hat{\Psi}_{n_f}$;
  Assign the obtained values into the corresponding terms of the event matrix $\mathbf{A}_{[n_f+1]}$: $\mathbf{A}_{[n_f+1]}(\psi) \leftarrow \Pr(C|\psi), \forall \psi \in \hat{\Psi}_{n_f}$;
  Run Algorithm 1 to generate the next event matrix: $\mathbf{A}_{[n_f+1]} \leftarrow$ `ExpandEventMatrix`$(\mathbf{A}_{[n_f]})$;
end

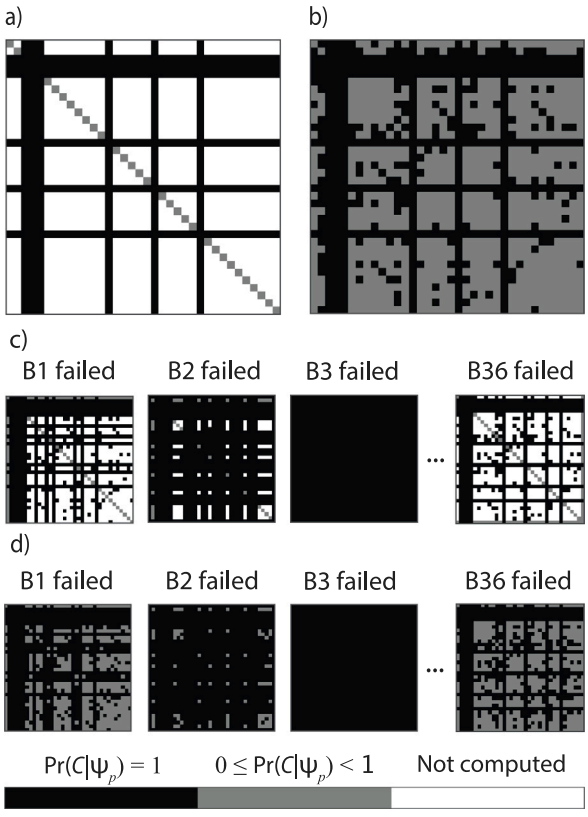

Fig. C.15. Sequential development of the event matrix **A** for the bracing BC1: (a) $N \times N$ matrix $\mathbf{A}_{[2]}$ ($N = 36$) after computing the N 1-member failure combinations, which correspond to the diagonal; (b) Matrix $\mathbf{A}_{[2]}$ after computing the 435 remaining 2-members failure combinations, which correspond to the unique white spaces of the matrix $\mathbf{A}_{[2]}$ in (a); (c) Slices of the $N \times N \times N$ matrix $\mathbf{A}_{[3]}$ using the information from all 2-members failure combinations; (d) Slices of the $N \times N \times N$ matrix $\mathbf{A}_{[3]}$ after assessing the 3-members failure combinations.

By way of example, the three first event matrices of BC1 are shown in Fig. C.15. At a given step of the truncation algorithm, the terms of an event matrix $\mathbf{A}_{[n_f]}$ are deterioration states that (1) have not yet been computed, (2) are associated with a probability of failure smaller than one, or (3) are associated with a probability of failure of one. These three possibilities are represented in the figure as white, grey and black squares, respectively.

References

[1] Martindale SG, Wirsching PH. Reliability-based progressive fatigue collapse. J Struct Eng 1983;109(8):1792–811. http://dx.doi.org/10.1061/(ASCE)0733-9445(1983)109:8(1792).

[2] Walsh C. Offshore wind in europe. key trends and statistics 2019. techreport, Wind Europe; 2019, URL https://windeurope.org/wp-content/uploads/files/about-wind/statistics/WindEurope-Annual-Offshore-Statistics-2019.pdf.

[3] Schafhirt S, Zwick D, Muskulus M. Two-stage local optimization of lattice type support structures for offshore wind turbines. Ocean Eng 2016;117:163–73. http://dx.doi.org/10.1016/j.oceaneng.2016.03.035.

[4] Straub D, Havbro Faber M. Risk based acceptance criteria for joints subject to fatigue deterioration. J Offshore Mech Arct Eng 2005;127:150–7. http://dx.doi.org/10.1115/1.1894412.

[5] Straub D, Der Kiureghian A. Reliability acceptance criteria for deteriorating elements of structural systems. J Struct Eng 2011;137(12):1573–82. http://dx.doi.org/10.1061/(ASCE)ST.1943-541X.0000425.

[6] Straub D, Schneider R, Bismut E, Kim H-J. Reliability analysis of deteriorating structural systems. Struct Saf 2020;82:101877. http://dx.doi.org/10.1016/j.strusafe.2019.101877.

[7] Moan T. Recent research and development relating to platform requalification. J Offshore Mech Arctic Eng 2000;122(1):20–32. http://dx.doi.org/10.1115/1.533720.

[8] Ronalds B, Pinna R, Ryan S, Riordan J, Radic T, Cole G, et al. Jacket reliability design considering interacting limit states. In: International conference on offshore mechanics and arctic engineering. no. OMAE2003-37044. 2003. p. 29–40.

[9] Moan T. Reliability-based management of inspection, maintenance and repair of offshore structures. Struct Infrastruct Eng 2005;1(1):33–62. http://dx.doi.org/10.1080/15732470412331289314.

[10] Agusta A, Leira BJ, Thöns S. Value of information-based risk and fatigue management for offshore structures. J Struct Integr Maint 2020;5(2):127–41. http://dx.doi.org/10.1080/24705314.2020.1729659.

[11] Moan T. Target levels for reliability-based assessment of offshore structures during design and operation. Offshore Technol Rep OTO 2002;60:2002.

[12] Shetty N. System reliability of fixed offshore structures under fatigue deterioration [Ph.D. thesis], Imperial College London; 1992.

[13] Dalane JI. System reliability in design and maintenance of fixed offshore structures [Ph.D. thesis], Trondheim: Norwegian Institute of Technology; 1993.

[14] Maljaars J, Vrouwenvelder ACWM. Probabilistic fatigue life updating accounting for inspections of multiple critical locations. Int J Fatigue 2014;68:24–37. http://dx.doi.org/10.1016/j.ijfatigue.2014.06.011.

[15] DNV-GL. Fatigue design of offshore steel structures. Recommended Practice DNVGL-RP-C203, DNV-GL; 2016.

[16] NORSOK. Design of steel structures. Standard N-004, Lysaker, Norway: Standards Norway; 2004.

[17] Gharaibeh ES, Frangopol DM, Onoufriou T. Reliability-based importance assessment of structural members with applications to complex structures. Comput Struct 2002;80(12):1113–31. http://dx.doi.org/10.1016/S0045-7949(02)00070-6.

[18] Kim D-S, Ok S-Y, Song J, Koh H-M. System reliability analysis using dominant failure modes identified by selective searching technique. Reliab Eng Syst Saf 2013;119:316–31. http://dx.doi.org/10.1016/j.ress.2013.02.007.

[19] ISO. Petroleum and natural gas industries — fixed steel offshore structures. Standard ISO 19902:2007, Geneva, Switzerland: International Organization for Standardization; 2007.

[20] Vugts JH. Handbook of bottom founded offshore structures: Part 1. General features of offshore structures and theoretical background, vol. 1. Eburon Uitgeverij BV; 2013.

[21] Efthymiou M, van de Graaf JW, Tromans PS, Hines IM. Reliability-based criteria for fixed steel offshore platforms. J Offshore Mech Arct Eng 1997;119(2):120–4. http://dx.doi.org/10.1115/1.2829053, arXiv:https://asmedigitalcollection.asme.org/offshoremechanics/article-pdf/119/2/120/5695616/120_1.pdf.

[22] Efthymiou M, van de Graaf JW. Reliability and (re)assessment of fixed steel structures. In: International conference on offshore mechanics and arctic engineering. no. OMAE2011-50253. 2011. p. 745–754.

[23] Stahl B, Aune S, Gebara JM, Cornell CA. Acceptance criteria for offshore platforms. J Offshore Mech Arctic Eng 2000;122(3):153–6.

[24] Thoft-Christensen P, Murotsu Y. Application of structural systems reliability theory. Springer Science & Business Media; 2012.

[25] Thoft-Christensen P, Sørensen JD. Reliability of structural systems with correlated elements. Appl Math Model 1982;6(3):171–8.

[26] Dunnett CW, Sobel M. Approximations to the probability integral and certain percentage points of a multivariate analogue of student's t-distribution. Biometrika 1955;42(1/2):258–60.

[27] Daniels HE. The statistical theory of the strength of bundles of threads. Proc R Soc Lond Ser A Math Phys Sci 1945;183(995):405–35.

[28] Gollwitzer S, Rackwitz R. On the reliability of Daniels systems. Struct Saf 1990;7(2–4):229–43. http://dx.doi.org/10.1016/0167-4730(90)90072-W.

[29] Kirkemo F. Probabilistic strategy increases jacket in-service inspection efficiency. Offshore Inc Oilman 1990;50:46–7.

[30] Liu Y, Moses F. Bridge design with reserve and residual reliability constraints. Struct Saf 1991;11(1):29–42.

[31] Billington CJ, Bolt HM, Ward JK. Reserve, residual and ultimate strength analysis of offshore structures: State of the art review. In: International offshore and polar engineering conference. OnePetro; 1993.

[32] Ditlevsen O. Narrow reliability bounds for structural systems. J Struct Mech 1979;7(4):453–72. http://dx.doi.org/10.1080/03601217908905329.

[33] Wheeler JD, et al. Method for calculating forces produced by irregular waves. J Pet Technol 1970;22(03):359–67.

[34] Morison JR, Johnson JW, Schaaf SA, et al. The force exerted by surface waves on piles. J Pet Technol 1950;2(05):149–54.

[35] Søreide TH, Amdahl J, Eberg E, et al. USFOS - A Computer Program for Progressive Collapse Analysis of Steel Offshore Structures. Theory Manual. techreport, Trondheim, Norway: SINTEF; 1993.